Performance of a Two-Junction Array SIS-Mixer Operating Around 345 GHz

C. E. Honingh, G. de Lange, M. M. T. M. Dierichs, H. H. A. Schaeffer, Th. de Graauw, and T. M. Klapwijk

Abstract—**We have made a detailed study of the gain and noise of a SIS heterodyne receiver at 345 GHz. As mixing element we use an array of two Nb-Al_2O_3-Nb SIS junctions in series. The array is operated in a waveguide mount with a backshort and an E-plane tuner. The best receiver noise temperature achieved is 140 K DSB. The embedding impedances were determined by fitting theory to the measured pumped curves. High-quality fits are obtained which constitute the first detailed test of the Tucker-theory at frequencies above 300 GHz. The impedances found by this method are in very good agreement with impedances measured in a scale model at 3.3 GHz. From these embedding impedances gain and noise of the mixer were calculated over a full bias range using the Tucker theory in the three-port low IF approximation. The calculated values are compared to mixer gain and noise as obtained from receiver measurements. The observed dependence of mixer gain and noise on bias voltage, pump power and embedding impedance is in good agreement with theory. However the absolute value of the measured gain is a factor .45 ± 0.05 lower than calculated. The measured mixer noise is approximately two quanta, 38 ± 10 K, higher than calculated. These discrepancies appear to be independent of the bias parameters of the mixer.**

I. Introduction

THE PERFORMANCE of SIS quasiparticle mixers [1] has surpassed that of other techniques for heterodyne detection in the frequency range up to 750 GHz [2], [3]. This progress has been largely due to an improvement of SIS junction technology and impedance matching techniques. Quantum limited performance has been demonstrated in the lower part of the spectrum, most recently at 100 GHz [4]. Interest in this frequency range is largely motivated by submillimeter astronomy, which eventually may require space qualified heterodyne receivers, presently under investigation at the European Space Agency (ESA). Although most initial results have been obtained with lead-alloy or tantalum-based junctions, more recent work uses almost invariably niobium based SIS junctions. This material is much more robust, both mechanically and thermally and the fabrication-technology has matured considerably.

To reach at submillimeter frequencies a performance comparable to that demonstrated at frequencies up to 100 GHz the radiation-coupling schemes successful at the lower frequencies must be scaled to the submillimeter wavelength domain. The quantum impedances of the quasiparticle currents are then fully accessible by tuning and quantum limited mixer performance can be expected. The typical junction response time, RC, times the frequency lies in the range 4 to 10 for mixers that have shown optimum performance (R is the junction normal state resistance and C the junction capacitance). Operating at higher frequencies requires a smaller RC-product, which can only be achieved with a thinner tunnel barrier i.e. a higher current density. Matching requirements at RF as well as IF-frequencies lead to a demand for junction areas around 1 μm^2.

Junction areas of about 1 μm^2 size are at the limit of what can be achieved with standard photolithography. Although smaller sizes can be made with electron-beam lithography the use of high-performance photolithography holds its attractions because of its higher fabrication throughput. As has been argued at an early stage of SIS-mixer development putting a number of junctions in series may alleviate the restrictions on the size of the junctions compared to those for a single junction [5], [6].

In this paper we report on a study of a waveguide-mixer operating at 345 GHz equipped with an array of two Nb/Al_2O_3/Nb junctions in series. Good receiver noise temperatures (140 K, double-side band) are obtained, which are comparable with results found elsewhere [7], [8]. Assuming quantum limited performance of the junctions array however would lead to a system temperature well below 100 K. To assess this difference, we make a full analysis of the array using the Tucker-theory. Embedding impedances are determined at the local-oscillator frequency and at both sideband frequencies. High-quality fits are obtained which constitute the first detailed test of the Tucker-theory at frequencies above 100 GHz. Gain and noise are calculated based on the measured embedding parameters over the full bias range. These results are compared with measured results. To extract the mixer parameters accurately from the receiver performance we measured the transmission loss of the IR-filter, the dewar-window and the beamsplitter in front of the mixer with a Fourier Transform Spectrometer (FTS). Moreover we calibrated the IF-stage of the mixer in situ, to make sure that we included all the contributions of cable/connector losses, and do all the calculations with the actual performance of the IF-system.

Manuscript revised October 14, 1992.

C. E. Honingh, H. H. A. Schaeffer, and Th. de Graauw are with the Space Research Organization of the Netherlands (S.R.O.N.) Landleven 12, 9747 AD Groningen, The Netherlands.

G. de Lange, M. M. T. M. Dierichs, and T. M. Klapwijk are with the Department of Applied Physics and Materials Science Centre, University of Groningen, Nijenborg 4, 9747 A. G. Groningen, The Netherlands.

IEEE Log Number 9206309.

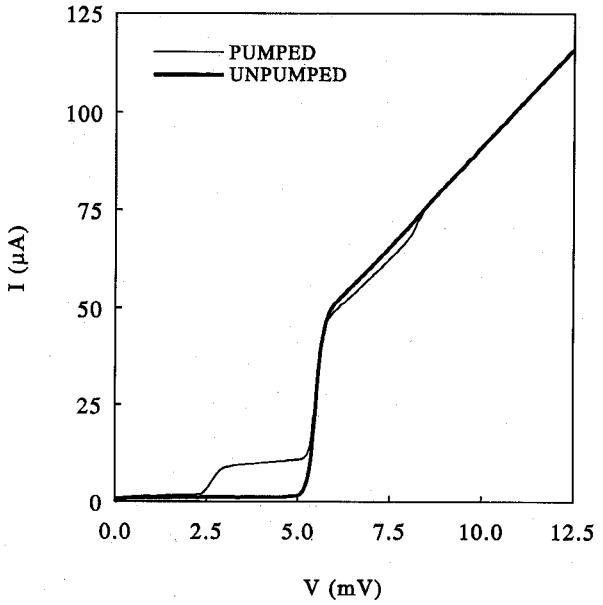

Fig. 1. Measured unpumped I,V-characteristic of the two junctions array used in these measurements. Each junction has an area of 0.8 μm^2. The pumped curve is taken at 350 GHz, with the tuner position and the LO-power set for optimum mixer performance.

II. Receiver Description

A. Junction Characteristics

An array of two Nb/Al_2O_3/Nb junctions in series is used. The junctions are fabricated on fused quartz substrates using the trilayer-approach first introduced by Gurvitch *et al.* [9]. Junctions are patterned photolithographically. Details of the fabrication are given by Dierichs *et al.* [10].

The majority of the experiments reported here were performed on a single sample of two junctions in series. The area of each junction is $0.9 \pm 0.1 \mu m^2$ and its normal state resistance is $54\,\Omega$. An unpumped I,V-curve of the array is shown in Fig. 1 together with a pumped curve at pump frequency 350 GHz. The junction, after mounting in the mixerblock, has been thermally cycled at least 30 times over a period of 4 months without any noticeable change in the current-voltage characteristic.

The dc-Josephson-effect is suppressed by a magnetic field generated by two coils in a Helmholtz configuration with its axis parallel to the plane of the junction.

B. Receiver Components and Measurement Set Up

A block diagram of the receiver system is given in Fig. 2. The dewar window (receiver part I) is made of 1.5 mm thick high-density polyethylene (HDP) and a fused quartz plan parallel plate (230 μm) is used as a resonant IR-filter (part II) at the 77K shield of the dewar. A cold lens is mounted directly onto the horn of the mixerblock and adjusted for optimum position at room temperature, using a bismuth bolometer as a detector in the block.

The mixer block has been described elsewhere [11]. Both tuners we use are adjustable non-contacting shorts. Scale model measurements at a frequency of 3.3 GHz have shown

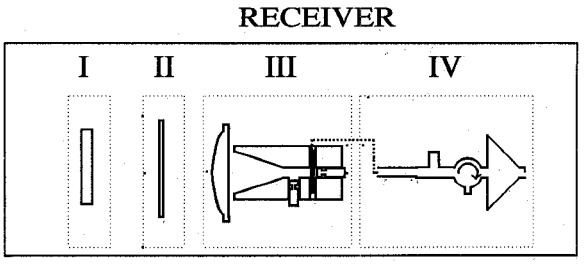

Fig. 2. Diagram of the receiver. Receiver-unit I is the dewar window at 300 K. Receiver units II, III and IV are located inside the dewar. II is the RF-filter at 77 K, III is the mixer, with lens-horns combination included and IV is the IF-chain.

that the tuning arrangement provides adequate matching for all relevant frequencies for virtually all practical junctions. Limits to the tuning range are mainly imposed by the losses in the tuning arrangement. Those are difficult to predict and depend mainly on the quality of the waveguide and the tuners.

In most measurements we used a 500–50 Ω matching transformer at the intermediate frequency (IF), with a bandwidth of 200 MHz around 1.4 GHz. The dc-bias is applied through an ordinary commercial bias-T and an isolator is used between the bias-T and the input of the first amplifer. The first amplifier after the mixer is a cooled HEMT amplifier (Berkshire Technologies) with a specified gain of 40 dB (1.2 - 1.7 GHz) and a specified noise temperature of 2 K.

The basic measurement set-up is fairly simple. Signals from the calibration source and the carcinotron local oscillator are combined at the receiver with a Kapton- beamsplitter. The LO-power transmitted by the beamsplitter is monitored with a Golay cell. We use an blackbody radiator at two known temperatures (295 K ,77 K) as calibrated input signal. The power output from this source is calculated using Planck's law. The signal power incident on the mixer is calculated taking into account the transmission of the beamsplitter, the dewar window and the filter, as measured separately with a FTS.

The IF-output power is measured as a function of biasvoltage in a bandwidth of 80 MHz by a commercial HP-power meter.

III. Impedance of the Junction Environment

The performance of the mixer is to a large extent determined by the electromagnetic environment of the SIS junction. A scale model of the mixer block has been used for the design and verification of its various components. Measurements at 3.3 GHz done with a standard network analyzer give the part of the embedding admittance indicated in Fig. 3 as Y_m. This part contains information about the waveguide, the tuners, the RF-filters and the metallization leading to the junction. The total embedding admittance of the junctions (Y_{emb}) is found by adding the geometrical capacitance of the junction array (Y_{cg}) in parallel to Y_m.

We also determined the embedding admittance of the actual mixer. By a careful analysis of the measured pumped I, V-curves we find three parameters which completely characterize the embedding circuit and the incident LO-power. These three parameters are $G_{\rm emb}$ and $B_{\rm emb}$, the real and imaginary part

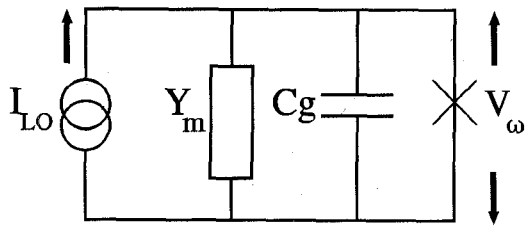

Fig. 3. The Norton equivalent of the embedding circuit seen by the SIS array. Y_m is the admittance measured in the scale model, Cg is the geometrical capacitance of the junction. $I_{\rm LO}$ represents the LO input power and $V\omega$ is the RF-voltage over the junction array, depicted by a cross.

of the total embedding impedance ($Y_{\rm emb}$) and I_{LO}, indicated in Fig. 3, which is an complex current source representing the incident LO-power. To accurately relate the measured pumped I,V-curves with theoretical curves various strategies have been used in the past. We have used the computerized voltage match method first introduced by Skalare [12].

In this method first the RF-voltage over the pumped junction (V_ω) is calculated at every biaspoint, using the umpumped I,V-curve measured under the same conditions.

The quantities in Fig. 3. are related through the network theorem:

$$|I_{\rm LO}|^2 = (I_\omega(V,V_\omega) + G_{\rm emb}V_\omega(V))^2 + (I'_\omega(V,V_\omega) + B_{\rm emb}V_\omega(V))^2 \qquad (1)$$

Knowing $V_\omega(V)$, the in phase ($I_\omega(V,V_\omega)$ and out of phase ($I'_\omega(V,V_\omega)$ RF-current through the junctions can be calculated from the expressions given in [1]. Using the fact that (1) must hold for all bias points $G_{\rm emb}$, $B_{\rm emb}$ and $|I_{LO}|$ are determined. For the fitting procedure we select mainly bias points on the first and second photon step below the gap voltage, because there the change of RF-current with bias voltage is strongest. Moreover the first deviations from the theory occur above the gap voltage. In the calculation the array of two junctions in series has been treated as a single junction with two times the gap voltage of one junction, assuming two identical component junctions.

In Fig. 4 the optimum calculated I,V-curve is compared with a measured I,V curve for an arbitrary value of pump power for two different embedding circuits. The figure of the RF-voltage across the junction illustrates the very good agreement between theory and measurement, especially below the gap voltage. Fits of comparable quality are reached for all relevant frequencies and for most pump powers. Deviations are found mainly at high power levels and they appear first above the energy gap. At tuning conditions close to the edge of the Smith Chart, illustrated in Fig. 5, high power levels are needed to get a well developed pump step. A decrease of the gap is then observed which depends on the dc-current through the junction and the theory is no longer applicable.

We have repeated the measurements several times to determine the variations in the values of the admittances. It turned out that the estimated value for $B_{\rm emb}$ did not vary more than 10% in between different fits at a data point with the same nominal embedding impedance. In the case of more capacitive embedding circuits the values for $G_{\rm emb}$ and $|I_{\rm LO}|$

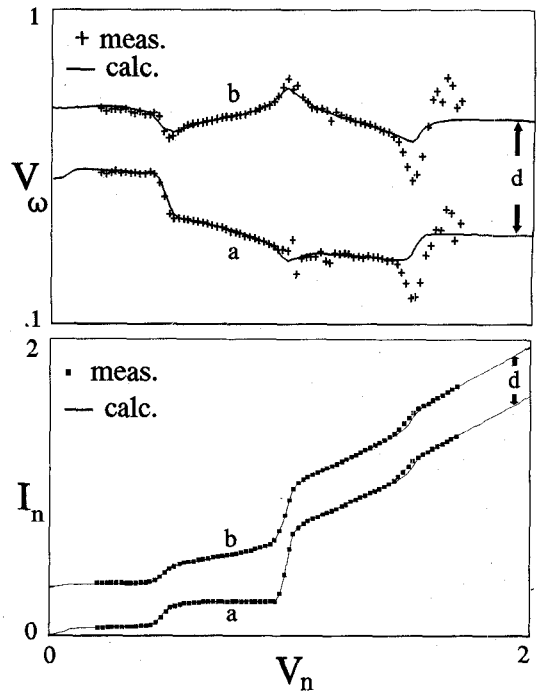

Fig. 4. Comparison between measured (+, ■) and calculated (—) RF-voltage and dc-current of the junction array as a function of bias voltage. The bias voltage is normalized to two times the gap voltage of one junction, and the normal state resistance of the junction is normalized to one. The curves for two different embedding admittances are vertically displaced by a distance d. The values voor $Y_{\rm emb}$, normalized to 1/110 Ω, 1.66–0.33i for curves (a) and 0.99 ± 2.15i for curves b.

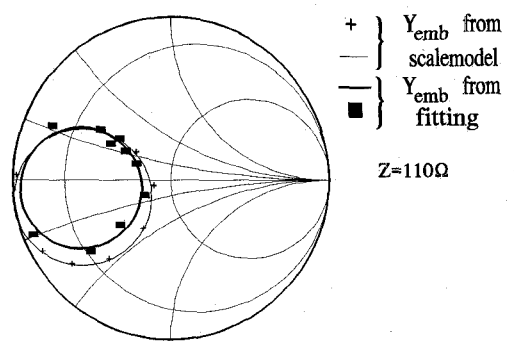

Fig. 5. The embedding admittances obtained from fitting the pumped curves (■) at different backshort positions using the same optimum E-plane tuner position. The smaller circle is a best fit through these admittance points. The bigger circle (-+-) is the result from the scale model measurement at a corresponding E-plane tuner position, with the junction geometrical capacitance added in parallel. 50 fF/ μm^2 is taken for the specific capacitance of the tunnel barrier.

however, which are directly related through the pump power, can vary up a factor of two. Because we register the input pump power we can relate pumped IV-curves at a different embedding impedances but at the same power level. Knowing the power level from fits at other embedding points gives an extra constraint besides (1), for $G_{\rm emb}$ and $|I_{\rm LO}|$, improving the accuracy of the fitted the embedding impedance.

To check the reliability of the data and to compare with the designed embedding, the values for $G_{\rm emb}$ and $B_{\rm emb}$ have been determined at various backshort settings, using the same optimum value for the E-plane tuner position. If the backshort

is lossless the admittances at different backshort settings lie on a circle in the Smith Chart. In Fig. 5 the smaller circle is a best estimate through the fitted embedding impedances which are marked by a ■-sign. The points in the highly capacitive area of the Smith Chart are all the result of repeated fitting, using the pump-power constraints. The admittances determined from the scale model measurements at an equivalent E-plane tuner setting are also shown in Fig. 5, indicated by th

e large circle marked with + signs. The good agreement between the designed embedding impedance from the scale model at 3.3 GHz and the embedding impedance measured in the actual mixer at 346 GHz would lead to the conclusion that the loss in the tuning is small. For the situation shown in Fig. 5 the distance between the edge of the Smith chart and the circle obtained from the data leads to an estimated loss of less than 1 dB.

IV. Mixer Theory

Our experimental results will be compared with the quantum theory of mixing [1]. A three-port mixer model is used i.e., currents that are generated at the first harmonic and higher harmonics are assumed short-circuited by the junction geometrical capacitance. This is a reasonable assumption for our junctions with $\omega RC = 5$.

To calculate the mixer performance the small signal voltages (v_i) produces across the junction at the three relevant frequencies (i) are taken to be the response to three current generators (i_i), which represent the incoming signal at each of these frequencies. They are linearly related by the 3 × 3 conversion matrix Z, taken from [1]:

$$Z = \begin{bmatrix} Y_{11} + Y_{usb} & Y_{10} & Y_{1-1} \\ Y_{01} & Y_{00} + Y_L & Y_{0-1} \\ Y_{-11} & Y_{-10} & Y_{-1-1} + Y_{lsb}* \end{bmatrix}^{-1} \quad (2)$$

The Y_{ij} elements characterise the junction array at a certain bias condition, which is determined by the LO power and the LO frequency, the embedding impedance at that frequency and the dc-bisasvoltage. The terms added to the diagonal elements of the matrix are the terminating admittances at the upper side band (usb) frequency ($i = 1$), the intermediate (L) frequency ($i = 0$), and the lower side band (lsb) frequency ($i = -1$) input port of the mixer.

The impedances at the LO frequency and at both side band frequencies differ significantly as is clearly illustrated in Fig. 6, where pumped I,V-curves are shown for different frequencies but fixed tuner setting. Clearly, the slope at the first photon-induced step is strongly effected by a frequency-change of 1.4 GHz. The impedances are determined with the fitting procedure outlined in Section III, and agree again well with what would be expected from the design. A separate reflection measurement at the IF port of the mixer with a standard (calibrated) network analyser at low power (−65 dBm) showed that the imaginary part of the IF load admittance is negligible between 1-2 GHz. So in the calculations we use $Y_L = G_L = (500\,\Omega)^{-1}$.

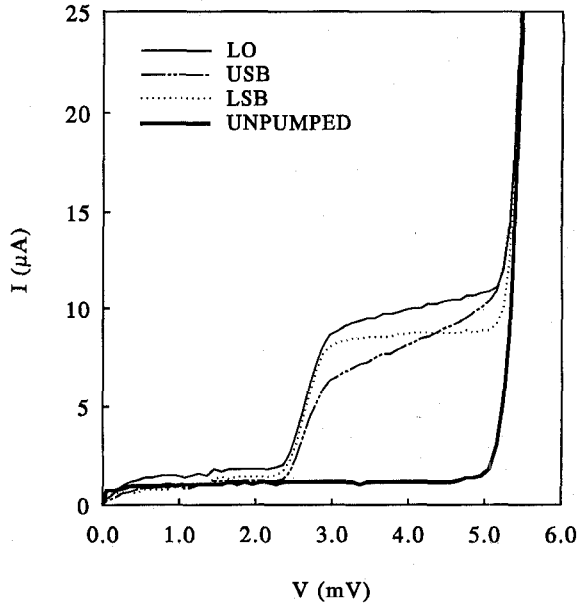

Fig. 6. Magnification of the DC I,V-curve from Fig. 1. Besides the pumped curve at the LO-frequency (352 GHz (LO)), curves at 350.6 GHz (LSB) and at 353.4 GHz (USB) are given, at the same input RF-power and the same tuner positions.

Using (2), with $\mathrm{Re}(Y_{\mathrm{usb}})$ is the real part of the embedding impedance at the usb frequency and $\mathrm{Re}(Y_{\mathrm{lsb}})$ is the same at the lsb frequency, the gain of the mixer is given by

$$Gm(V, V_\omega) = 4G_L\,(\mathrm{Re}\,(Y_{\mathrm{usb}})|Z_{01}(V, V_\omega)|^2 + \mathrm{Re}\,(Y_{\mathrm{lsb}})|Z_{0-1}(V, V_\omega)|^2) \quad (3)$$

The total IF output power of the receiver as a function of bias voltage, in a bandwidth B, at an input power P_{in} is given by

$$P_{\mathrm{out}}(V, V_\omega) = G_{\mathrm{IF}}\,[P_S(V, V_\omega) + P_Q(V, V_\omega) + A_{\mathrm{ex}} Gm(V, V_\omega)\,(P_{\mathrm{in}} + P_{\mathrm{ex}}) + \ldots + kB(T_{\mathrm{isol}}|\Gamma_{\mathrm{IF}}(V, V_\omega)|^2 + T_{\mathrm{IF}})] \quad (4)$$

where G_{IF} is the gain of the IF-chain. $P_s\,(V)$ gives the output power due to the noise in the mixer generated by fluctuations in the tunneling current. The rms expectation value of this current fluctuation is calculated using the current correlation H-matrix formulation derived in [1]. $P_Q(V)$ is the contribution due to the vacuum fluctuations following from the rigorous analysis of Wengler and Woody [13]. This contribution is comes down to the coupled output power of approximately half a fluxquant input power at each side band.

The third term, which gives the contribution due to the incident radiation (P_{in}) is multiplied by an extra factor A_{ex}, to implement a correction based on the measured mixer gain. Also an extra input power term P_{ex} is added. It will be shown later (Section VI) that extra noise present in the measured data can be added consistently in (4) as P_{ex}. The fourth term in (4) represents the contribution of the IF stage of the receiver. It is split in a bias voltage dependent part and a constant part where T_{IF} is the noise temperature of the amplifier. The voltage

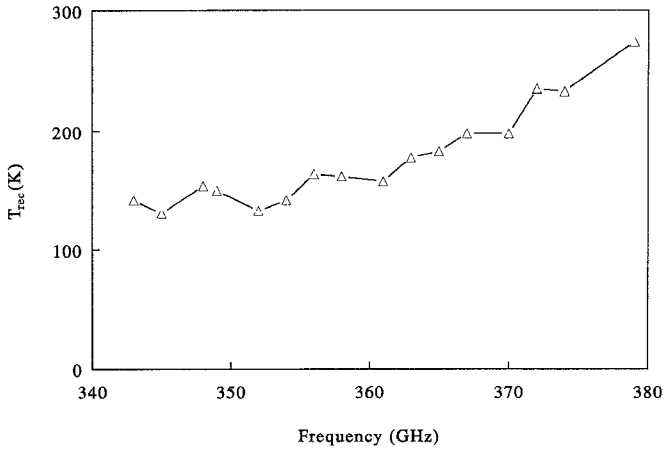

Fig. 7. Measured receiver noise temperature obtained from a hot/cold measurement. The cold load temperature is corrected for the contribution of the beamsplitter reflection/transmission ratio of 89%.

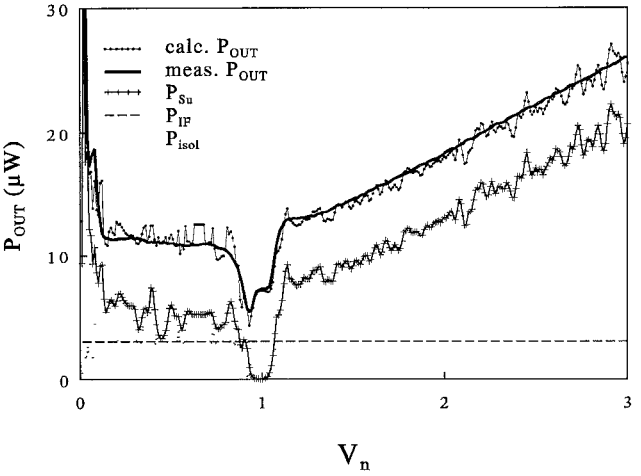

Fig. 8. IF output power of the unpumped junction array as a function of bias voltage, measured (solid fat line) and calculated (-•-). The various contributions to the total calculated result are the shot noise and thermal noise of the junction array P_{Su} (-+-), the thermal noise reflected at the IF-port of the mixer P_{isol} (. .), and the contribution of the IF-amplifier P_{IF} (-\thinspace-), all given as a function of bias voltage.

dependent part represents the thermal noise power reflected from the IF-port of the mixer. $\Gamma_{\mathrm{IF}}(V)$ is the bias voltage dependent voltage reflection coefficient due to the mismatch between $\mathrm{Re}(Y_L)$ and $dI_{\mathrm{do}}/dV(V)$.

V. Measured Performance

A. System Performance

The optimum receiver noise temperature as a function of frequency is given in Fig. 7. At each frequency the optimum setting of the mixer was determined by maximizing the IF response to a chopped hot (300 K)/cold(77 K) load, which maximizes the sum of the coupled gain of both side bands. The position of both tuners, the dc-biasvoltage and the LO-power were optimized iteratively. We found that the optimum gain did not depend very strongly on the LO-power level and was usually found at a bias voltage a little higher than the middle of the first photon step. The temperatures in Fig. 7 are corrected for the transmission of the beamsplitter, which is 89 ± 1%.

A magnetic field of approximately 300 Gauss is applied at all measurements, carefully adjusted to reach the second minimum of the Fraunhofer diffraction pattern of the super-current as a function of magnetic field. The two junctions are sufficiently identical to suppress all Josephson effects visible at the IF output. At the field strength used the current rise at the gap is unaffected, showing that the density of states is not changed by the magnetic field.

All measurements are performed at a liquid helium bath temperature of 4.2 K. The mixer itself is at a slightly (< 0.5 K) elevated temperature mounted in vacuum to the bottom of the helium vessel.

B. Calibration of the IF-system

To determine the gain and noise of the IF-system (receiver section IV in Fig. 2) the unpumped junction array is used as a biasvoltage dependent calibration noise source [14].

Assuming that N junctions series are N uncorrelated sources of noise, the output power of the unpumped junction array, coupled to the IF-amplifier load Y_L, as a function of bias voltage is given by [15].

$$P_{Su}(V) = \frac{2eB}{N}\,\mathrm{Re}(Y_L)I_{\mathrm{dc}}(V) \cdot \coth\left(\frac{eV}{2kT}\right)\left(\frac{dI_{\mathrm{dc}}}{dV}(V) + \mathrm{Re}(Y_L)\right)^{-2} \quad (5)$$

where e is the electron charge, k is the Boltzman constant and $I_{\mathrm{DC}}(V)$ is the DC-IV characteristic of the array at physical temperature T. B is the output bandwidth.

A typical registration of the IF output power as a function of biasvoltage is given in Fig. 8. The IF output power has been fitted to (4), with $Gm(V) = 0$ and $P_S(v) = P_{Su}(V)$. From the fit the gain and noise contribution of the IF system are obtained.

The gain is determined with an accuracy of ± 0.2 dB from the slope of the curve above about two times the gap voltage and is in good agreement with values obtained from separate measurements. The noise temperature of the amplifier and the isolator contribution are then determined from the absolute value of the power. Both contributions can be separated easily due to the bias voltage dependence of $\Gamma_{\mathrm{IF}}(V)$. T_{IF} is slightly higher than the manufacturer specified (3 ± 0.5 K) and for T_{isol} we find 4.5 K. If we use an IF transformer we find $T_{\mathrm{isol}} = 5.5$ K, possibly due to a worse isolator performance. We have no indication that the noise behaviour of the IF-amplifier changes as a result of the high source impedances at biasvoltages below the gap.

C. Comparison of Measured and Calculated Mixer Performance

The IF output power is measured as a function of bias voltage, subsequently with a 295 K and a 77 K blackbody source as input signal. Corrected for the transmission (A) of

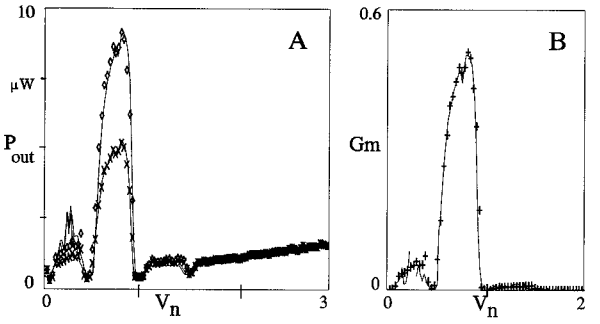

Fig. 9. (a) The IF output power from a pumped junction, both with a hot (O) and a cold (X) input load at the RF-port at the optimum tuning point. The drawn curves are measured, the marked ones are calculated, using the measured gain of Fig. 9(b), and adding extra input power on the mixer, at both the hot and the cold load, equivalent to a blackbody of 77 K. (b) The mixer gain at the optimum tuning point as obtained from the subtraction of the hot and cold load measurements (solid line) and calculated points (+) from the three port mixer theory. The calculated values have been multiplied by .45 to obtain the agreement as shown.

the beam splitter ($A = 89 \pm 1\%$), the dewar window (I, $A = 95 \pm 1\%$) and the RF-filter (II, $A = 95\% \pm 1\%$) at 77 K, see Fig. 2, the input temperatures on the mixer become 275 K and 101 K. It is assumed that the dewar window has a temperature of 285 K and the RF-filter has a temperature of 80 K. The lens/horn combination is taken to be part of the mixer.

D. Mixer Gain

Using the gain of the IF-chain determined in section V;B the gain of the mixer is obtained from the subtraction of the two measurements with the hot and cold load. The two measurements are shown in Fig. 9(a) and the gain is shown in Fig. 9(b), both as a function of bias voltage at the optimum turning point. The mixer gain is also calculated from Eq. 3 using the embedding admittances fitted to the pumped curves. The values used are $Y_{\mathrm{LO}} = 1.8 + 0.52\mathrm{i}$, $Y_{\mathrm{usb}} = 0.54 + 0.88\mathrm{i}$ and $Y_{\mathrm{lsb}} = 2.68 - 0.732\mathrm{i}$, all normalized to $1/(110\ \Omega)$. This calculated gain is represented by the plusses in Fig. 9(b). To get the good agreement between the two curves the calculated gain had to be multiplied by a constant factor 0.45. It turned out that also for most other, non optimum tuning points, approximately the same discrepancy existed. This gives for the extra factor in (4) $A_{\mathrm{ex}} = 0.45 \pm 0.05$. Only for the most inductive tuning points the factor approached .25.

To investigate the behavior of A_{ex} further we compared calculation and measurement on the variation of mixer gain with backshort position. Upon moving the backshort the embedding admittance presented to the junction repeats each 1/2 lambda guide of the pump frequency (tuning cycle). While the embedding impedance at the local oscillator frequency is the same at corresponding points in the second (and subsequent) tuning cycle(s), the admittances at the side band frequencies change. This causes the mixer gain to decrease while moving the backshort away from the junction.

In Fig. 10 measured curves for three pairs of backshort positions (I–III) in the first and second tuning cycle reckoning from the junction, are given by the drawn lines. Point II is about the optimum tuning point of the mixer, and points

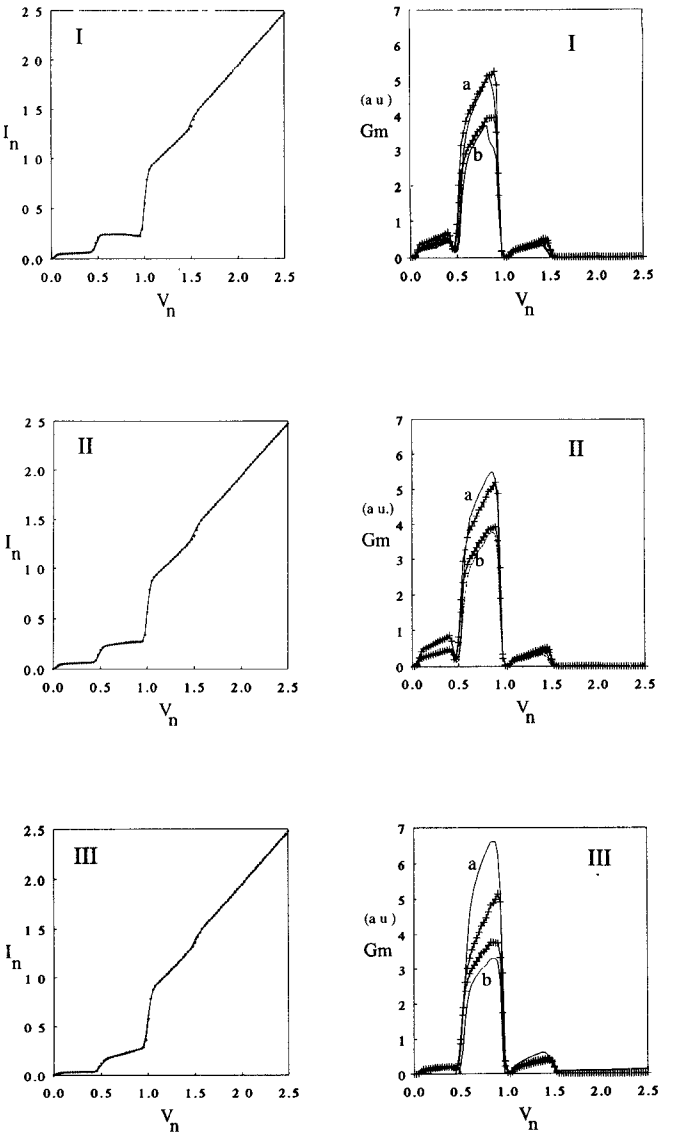

Fig. 10. Measured (—) and calculated (+, •) gain and corresponding pumped I,V-curves for the two subsequent backshort cycles of which the embedding impedances are given in Fig. 11.

I and III are displaced from the optimum in inductive and capacitive direction respectively. For all curves the pump power and the pump frequency are the same. It can be seen that the corresponding I,V-curves for both tuning cycles overlap, indicating very little loss in the waveguide. The mixer gain however clearly decreases.

The embedding admittances at the points I–III, as obtained from fitting, are indicated in Fig. 11 by a +-sign. The upper (#) and lower (•) sideband admittances for all three pairs of backshort positions in the first (a) and the second (b) tuning cycle are also indicated in Fig. 11. These admittances are not obtained from fitting pumped I,V-curves but from the scale model. Because of the error margin in the fitting, especially in the more capacitive region of the Smith Chart, the side band admittances in the first and second tuning cycle were not very well distinguished. They were however, within the error, equal to the admittances that followed from the scale model.

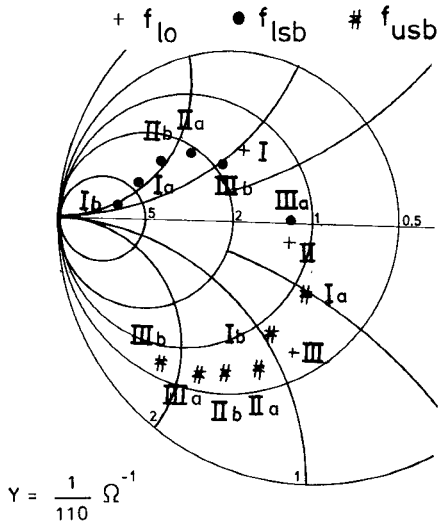

Fig. 11. Compression of the mixer gain with mixer bandwidth. Points (+) I, II, and III indicate three corresponding pairs of admittances with a different backshort settings at the same optimum E-plane tuner position. All three points are reached two times in two corresponding backshort settings (a and b), 1/2 lambda guide apart. The admittances at the upper (#) and lower (•) sideband frequencies that correspond to these six backshort settings are also given. The side band impedances are obtained from the scale model, the LO-impedances are fitted from pumped I,V-curves.

The pumped I,V-curves and the mixer gain calculated using the embedding impedances from Fig. 11 are also indicated in Fig. 10. To obtain the agreement with the measurements as shown, all calculated gains are multiplied with a constant factor $A_{ex} = 0.41$. The agreement at point I and II is very good, while the deviation in point III might very well be caused by the inaccuracy in the embedding admittance at the LO-frequency.

E. Mixer Noise

To match measured and calculated mixer gain we had to introduce the factor A_{ex} to (4). Using (4) in that form we found that, at the optimum tuning point, for P_{ex} a power equivalent to a blackbody radiating at 77 K was needed to give an agreement between measured and calculated IF-output power. In Fig. 9(a) the measured (+) and calculated (—) curves are given for a hot and a cold input load. To calculate the noise generated by the LO and the dc current through the junctions, the two junctions in series are regarded, as in the unpumped case, as two uncorrelated sources of noise by much the same arguments as Kerr [16]. In the calculation this is accomplished by replacing the junction array by one equivalent junction [1].

We determined the value of P_{ex} also for different bias and tuning conditions of the mixer. In general we found that all measurements were well described using a value for P_{ex} equivalent with a blackbody radiator at 85 ± 25 K.

VI. Discussion and Conclusions

The accurate knowledge of the embedding impedances allowed us to make a detailed comparison between theory and data. We used high quality, small area (1 μm^2) SIS-junctions (Fig. 1) with a normal state resistance of approximately 50 Ω. The embedding impedances have been designed and measured with a scale model. When we determined the actual embedding impedance at 350 GHz, we found that it agrees excellently with the designed embedding impedance (Fig. 5). We have seen no problem in the analysis from the fact that we used a two junction in series rather than one single junction. The dependence of the measured mixer gain on embedding impedances at the LO and the side band frequencies agreed very well with the predictions from the three port mixer theory, for an arbitrary LO-power value. (Fig. 9). This nice agreement between data and theory on the dependence of the bias parameters of the mixer offers no explanation for the observed discrepancies in the absolute values.

The discrepancy between the measured and calculated mixer gain is determined accurately. The noise terms do not play a role in the analysis so the main inaccuracies are due to the input power (6%) and the IF-gain (4%). We believe that the calibration of the IF-system (Sect. V-B) is accurate. It reproduces very well between separate measurements. A systematic error in the input power can be formed by the lens-horn combination. It has been tested separately outside the mixer dewar at room temperature. The beam pattern agrees with the calculations and a worst case estimate for its power loss, measured with two horns back to back is 15%. The beam has been checked at operating conditions and we are convinced that it couples fully to the hot/cold load. The power loss in the waveguide and the tuners is hard to determine but it seems lower than 15% judging from Fig. 5. These two contributions do not fully explain the observed discrepancy between theory and measurements. The discrepancy in gain however is constant over a large parameter space. This seems to point at some kind of systematic error, most likely in the measurement set up. We are presently investigating the cold lens and the IR-filter for arte-facts.

To find an explanation for the value of P_{ex} we ran some experimental tests on possible noise contributions not governed by theory. Small variations of the magnetic field that suppressed the dc-Josephson effect only caused spikes on the IF-output power and did not change the overall levels. In a test experiment possible noise from the LO-source at the side band frequencies was filtered by a high Q Fabry-Pérot filter, which again did not change the noise levels. We changed the beamsplitter, the RF-filter and the dewar window. All set-ups gave, within the error, the same results on mixer gain and noise.

Because we could not find an outside source for P_{ex}, we regard P_{ex} as an intrinsic extra noise contribution in the mixer. Since we attribute A_{ex} fully to an unknown loss at 4.2 K, in front of the mixer (lens, horn) or in the tuning arrangement, this means that we have to multiply P_{ex} by A_{ex} to find the extra mixer noise. It turns out that the product $P_{ex} \cdot A_{ex} = 38 \pm 10$ K over a large parameter space.

There is the possibility that the theory does not give correct predictions, especially since we use a series array of junctions. Results reported by other workers on this matter do not always agree. The accurate and detailed study by McGrath *et al.* [17] reports at 37 GHz that for junction I,V-characteristics where the voltage width of the current rise at the gap is smaller than

the pump frequency quasi particle step, theory and practice begin to deviate.

The gain figures as a function of backshort position in [4] show that in the regime where we are comparing data to theory, the measured gain is approximately 2 dB lower than calculated, although every precaution was made in this study to make an accurate comparison, and the measured noise in this paper is quantum limited. There are also however authors who reported good agreement [6], [18] on the gain, also for series arrays of junctions.

Results on mixer noise in literature are also not unambiguous. Crété *et al.* [19] found an unexplained amount of excess noise in measurements on various arrays of junctions with different numbers of elements. Pan *et al.* [20] however showed a well understood noise performance at 115 GHz using a two junction in series array. Also for single junction mixers the agreement is not always found [17] despite very systematic and accurate measurements.

We think it unlikely, as frequently mentioned at lower frequencies, that second harmonic responses are important. The second harmonic frequency is already above the gap frequency of Niobium. It is possible that the assumption that the noise of two junctions in series is uncorrelated is not right. If the noise is fully correlated the calculated mixer noise would be approximately 26 K higher, explaining almost the whole extra noise contribution. We plan to do the same noise measurements on a single junction mixer as soon as devices are available.

ACKNOWLEDGMENT

We thank J. J. Wezelman for technical assistance also in overtime, J. v. d. Kuur for assistance with programming work and helpful discussions, R. A. Panhuyzen for the realization of the masks and H. v. d. Stadt and A. Skalare for a careful reading of the manuscript. This research was supported by the Stichting Technische Wetenschappen (STW) and the European Space Agency under contract No. 7898/88/NL/PB(SC).

REFERENCES

[1] J. R. Tucker and M. J. Feldman, "Quantum detection at millimeter wavelengths," *Rev. Modern Phys.*, vol. 57, pp. 1055–1113, 1985.
[2] B. N. Ellison, P. L. Schaffer, W. Schaal, D. Vail, and R. E. Miller, "A 345 GHz SIS receiver for radio astronomy," *Int. J. of IR and MM Waves*, vol. 10, pp. 937–947, 1989.
[3] T. H. Büttgenbach, R. E. Miller, D. M. Wengler, D. M. Watson, and T. G. Phillips, "A broad-band low-noise SIS receiver for submillimeter astronomy," *IEEE Trans. Microwave Theory Tech.*, vol. 36, pp. 1720–1726, 1988.
[4] C. A. Mears, Qing Hu, P. L. Richards, A. H. Worsham, D. E. Prober and A. V. Räisänen, "Quantum limited quasiparticle mixers at 100 GHz," *IEEE Trans.Magn.*, vol. 27, pp. 3363–3369, 1991.
[5] P. L. Richards, T.-M. Shen, R. E. Harris, and F. L. Lloyd, "Quasi particle heterodyne mixing in SIS tunnel junctions," *Appl. Phys Lett.*, vol. 34, pp. 345–347, 1981.
[6] S. Rudner, M. J. Feldman, E. Kollberg, and T. Claeson, "SIS mixing with arrays at millimeter wave frequencies," *J. Appl. Phys.*, vol. 52, pp. 6366–6377, 1981.
[7] E. C. Sutton, W. C. Danchi, P. A. Jaminet, and R. H. Ono, "A superconducting tunnel junction receiver for 345 GHz," *Int. J. IR and MM Waves*, vol. 11, pp. 133–150, 1990.
[8] H. Rothermel, D. Billon-Pierron, and K. H. Gundlach, "An open structure mixer for 350 GHz," *Conf. Dig. 16th Int. Conf. Infrared Millimeter Waves*, pp. 135–136, 1991.
[9] M. Gurvitch, M. A. Washington, and H. A. Huggins, "High quality refractory Josephson tunnel junctions using thin aluminum layers," *Appl. Phys. Lett.*, vol. 42, pp. 472–479, 1983.
[10] M. M. T. M. Dierichs, R. A. Panhuyzen, C. E. Honingh, M. J. de Boer, and T. M. Klapwijk, "Sub-micron niobium junctions for submillimeter-wave mixers using optical lithography," *Applied Physics Letter*, vol. 62, pp. 774–777, 1993.
[11] C. E. Honingh, H. H. A. Schaeffer, Th. de Graauw, M. M. T. M. Dierichs and T. M. Klapwijk, "SIS mixing with Arrays of Nb-Al_2O_3-Nb Junctions," *Proc. Int Symp. on Space Terahertz Technology*, 1991, pp. 473–480.
[12] A. Skalare, "Determining embedding circuit parameters from dc measurements on quasiparticle mixers," *Int. J. of IR and MM Waves*, vol. 10, pp. 1339–1353, 1989.
[13] M. J. Wengler, and D. P. Woody, "Quantum noise in heterodyne detection," *IEEE J. Quantum Electron.*, vol. QE-23, pp. 613–622, 1987.
[14] V. Yu. Belitsky, V. P. Koshelets, I. L. Serpuchenko, M. A. Tarasov, L. V. Filippenko, and S. V. Shitov, "Superconducting tunnel junction noise generator and SIS mixers noise measurements," *European Microwave Conf.*, Budapest, Sept. 1990.
[15] J. R. Tucker, "Quantum limited detection in tunnel junction mixers," *IEEE J. Quantum Electron.*, vol. QE-15, pp. 1234–1257, 1979.
[16] A. R. Kerr, "Noise and Loss in Balanced and Subharmonically Pumped Mixers, Part 1-Theory," *IEEE Trans. Microwave Theory Tech.*, vol. MTT-27, pp. 938–950, 1979.
[17] W. R. McGrath, P. L. Richards, D. W. Face, D. E. Prober, and F. L. Lloyd, "Accurate experimental and theoretical comparisons between SIS mixers showing weak and strong quantum effects," *J. Appl. Phys.*, vol. 63, pp. 2479–2491, 1988.
[18] M. J. Feldman, S.-K. Pan, A. R. Kerr and A. Davidson, "SIS mixer analysis using a scale model," *IEEE Trans. Magn.*, vol. MAG-19, pp. 494–497, 1983.
[19] D. W. Crété, W. R. McGrath, P. L. Richards, and F. L. LLoyd, "Performance of arrays of SIS junctions in heterodyne mixers," *IEEE Trans. Microwave Theory Tech.*, vol. MTT-35, pp. 435–440, 1987.
[20] S.-K. Pan, M. J. Feldman, and A. R. Kerr, "Low noise 115 GHz receiver using superconducting tunnel junctions," *Appl. Phys. Lett.*, vol. 43, pp. 786–788, 1983.

C. E. Honingh, photograph and biography not available at the time of publication.

G. de Lange, photograph and biography not available at the time of publication.

M. M. T. M. Dierichs, photograph and biography not available at the time of publication.

H. H. A. Schaeffer, photograph and biography not available at the time of publication.

Th. de Graauw, photograph and biography not available at the time of publication.

T. M. Klapwijk, photograph and biography not available at the time of publication.